A new photometric and dynamical study of the eclipsing binary star HW Virginis

S. B. Brown-Sevilla, V. Nascimbeni, L. Borsato, L. Tartaglia, D. Nardiello, V. Granata, M. Libralato, M. Damasso, G. Piotto, D. Pollacco, et al.

▶ **To cite this version:**

S. B. Brown-Sevilla, V. Nascimbeni, L. Borsato, L. Tartaglia, D. Nardiello, et al.. A new photometric and dynamical study of the eclipsing binary star HW Virginis. Monthly Notices of the Royal Astronomical Society, 2021, 506, pp.2122-2135. ⟨10.1093/mnras/stab1843⟩. ⟨hal-03585937⟩

HAL Id: hal-03585937

https://hal.science/hal-03585937v1

Submitted on 20 Apr 2023

HAL is a multi-disciplinary open access archive for the deposit and dissemination of scientific research documents, whether they are published or not. The documents may come from teaching and research institutions in France or abroad, or from public or private research centers.

L'archive ouverte pluridisciplinaire **HAL**, est destinée au dépôt et à la diffusion de documents scientifiques de niveau recherche, publiés ou non, émanant des établissements d'enseignement et de recherche français ou étrangers, des laboratoires publics ou privés.

HAL Authorization

Monthly Notices of the ROYAL ASTRONOMICAL SOCIETY

MNRAS **506,** 2122–2135 (2021) https://doi.org/10.1093/mnras/stab1843
Advance Access publication 2021 July 2

A new photometric and dynamical study of the eclipsing binary star HW Virginis

S. B. Brown-Sevilla [1,2★†], V. Nascimbeni [2,3★], L. Borsato [2,3], L. Tartaglia,[3] D. Nardiello [3,4], V. Granata [2,3], M. Libralato [2,3,5], M. Damasso,[6] G. Piotto,[2,3] D. Pollacco,[7] R. G. West [7,8], L. S. Colombo,[2,3] A. Cunial,[2,3] G. Piazza[2] and F. Scaggiante[9]

[1]*Max-Planck Institute for Astronomy, Königstuhl 17, D-69117 Heidelberg, Germany*
[2]*Dipartimento di Fisica e Astronomia, Università degli Studi di Padova, Vicolo dell'Osservatorio 3, I-35122 Padova, Italy*
[3]*INAF – Osservatorio Astronomico di Padova, Vicolo dell'Osservatorio 5, I-35122 Padova, Italy*
[4]*LAM, Aix Marseille University, CNRS, CNES, UMR 7326, 13388 Marseille, France*
[5]*AURA for the European Space Agency (ESA), ESA Office, Space Telescope Science Institute, 3700 San Martin Drive, Baltimore, MD 21218, USA*
[6]*INAF – Osservatorio Astrofisico di Torino, Via Osservatorio 20, I-10025 Pino Torinese, Italy*
[7]*Department of Physics, University of Warwick, Gibbet Hill Road, Coventry CV4 7AL, UK*
[8]*Centre for Exoplanets and Habitability, University of Warwick, Gibbet Hill Road, Coventry CV4 7AL, UK*
[9]*Gruppo Astrofili Salese 'G. Galilei', I-30036 Santa Maria di Sala (VE), Italy*

Accepted 2021 June 24. Received 2021 June 22; in original form 2021 May 24

ABSTRACT

A growing number of eclipsing binary systems of the 'HW Virginis' (HW Vir) kind (i.e. composed by a subdwarf-B/O primary star and an M dwarf secondary) show variations in their orbital period, also called eclipse time variations (ETVs). Their physical origin is not yet known with certainty: While some ETVs have been claimed to arise from dynamical perturbations due to the presence of circumbinary planetary companions, other authors suggest that the Applegate effect or other unknown stellar mechanisms could be responsible for them. In this work, we present 28 unpublished high-precision light curves of one of the most controversial of these systems, the prototype HW Vir. We homogeneously analysed the new eclipse timings together with historical data obtained between 1983 and 2012, demonstrating that the planetary models previously claimed do not fit the new photometric data, besides being dynamically unstable. In an effort to find a new model able to fit all the available data, we developed a new approach based on a global-search genetic algorithm and eventually found two new distinct families of solutions that fit the observed timings very well, yet dynamically unstable at the 10^5-yr time-scale. This serves as a cautionary tale on the existence of formal solutions that apparently explain ETVs but are not physically meaningful, and on the need of carefully testing their stability. On the other hand, our data confirm the presence of an ETV on HW Vir that known stellar mechanisms are unable to explain, pushing towards further observing and modeling efforts.

Key words: binaries: eclipsing – stars: individual: HW Vir – planetary systems – planets and satellites: dynamical evolution and stability – techniques: photometric.

1 INTRODUCTION

The discovery of the first exoplanets by Wolszczan & Frail (1992) and Mayor & Queloz (1995) was the starting point to the detection of a great number of other planetary systems through different observing techniques. Although the majority of them have been found orbiting Sun-like stars (e.g. Petigura, Marcy & Howard 2015), there is an increasing number of exoplanets being discovered orbiting all kinds of stars (e.g. Gould et al. 2014; Gillon et al. 2017; Brewer et al. 2018). A particularly interesting case among them is represented by circumbinary planets, which orbit a binary system instead of a single star. These kinds of planets can be detected, among other techniques (such as transits, e.g. Kostov et al. 2016; radial velocity, e.g. Konacki et al. 2009; or light traveltime delay, e.g. Silvotti et al. 2018), by measuring and analysing changes in the orbital period of eclipsing binary stars, a dynamical method commonly known as eclipse time variations (ETVs; e.g. Sale et al. 2020). These variations have been observed in a wide range of binary systems, such as post-common envelope binaries, which exhibit modulation periods of a few tens of years (e.g. Bours et al. 2016). A possible mechanism to explain ETVs is the light traveltime effect (LTTE; also known as the Rømer effect), which refers to the combination of the motion of the stellar components with respect to the barycentre of the system due to the gravitational perturbation of additional bodies, with the finite speed of light (Irwin 1952).

Among the vast taxonomy of eclipsing binaries, the so-called 'HW Virginis' (HW Vir) systems have recently drawn the attention of astronomers. These systems are post-common envelope binaries

★ E-mail: brown@mpia.de (SBB-S); valerio.nascimbeni@inaf.it (VN)
† Member of the International Max-Planck Research School for Astronomy and Cosmic Physics at the University of Heidelberg (IMPRS-HD), Germany.

© 2021 The Author(s)
Published by Oxford University Press on behalf of Royal Astronomical Society

Downloaded from https://academic.oup.com/mnras/article/506/2/2122/6313312 by INIST-CNRS INSU user on 20 April 2023

composed of a subdwarf of spectral type O or B and a late-type main-sequence star, e.g. sdB + dM for the prototype. They have very short orbital periods (of the order of a few hours), and in a surprisingly high fraction of the cases, ETVs have been observed, typically from tens of seconds to several minutes of amplitude and semiregular modulations on long time-scales, from years to decades (see Heber 2016, for a detailed review on HW Vir systems). Different explanations have been proposed to interpret ETVs, usually based on two different effects or a combination of them: the LTTE effect caused by one or more unseen companions, and the so-called Applegate effect. The latter was first proposed by Applegate (1992), and it interprets the variations on the orbital period as a consequence of magnetic activity in one of the stars of the binary system (in the case of HW Vir, the main-sequence component). According to Applegate (1992), the distribution of the angular momentum in the active star changes as the star goes through its activity cycle. These variations on the angular momentum distribution induce a change in the gravitational quadrupole moment of the star (making it more or less oblate), which can cause perturbations in the orbit of the system and thus in the orbital period.

In this work, we analyse data from the prototypical HW Vir, a detached eclipsing binary system first identified as such by Menzies & Marang (1986). HW Vir has a very short period of 2.8 h, and its components have masses of 0.49 and 0.14 $M_{\odot}$, for the sdB and dM components, respectively (see Table 1 for the most recent parameters of HW Vir). Since its discovery, the system has been broadly studied due to its intrinsic characteristics and its striking period variations. A decrease in the orbital period of the system was first detected by Kilkenny, Marang & Menzies (1994), followed by Çakirli & Devlen (1999), who re-analysed the eclipse timings between 1984 and 1999 and concluded that LTTE was the most promising explanation for the observed period variations. They proposed that HW Vir was revolving about a third body with a period of 19 yr. Later on, further studies were performed (Wood & Saffer 1999; Kilkenny et al. 2000; Kiss et al. 2000) analysing the period variations with different techniques, without reaching a definitive explanation. Kilkenny, van Wyk & Marang (2003) presented new eclipse timings for HW Vir and confirmed the presence of a periodic LTTE term due to a third body in the system, a claim also supported by İbanoğlu et al. (2004).

Lee et al. (2009) presented new CCD photometry with an 8-yr baseline, and proposed that the linear term of the period decrease (dP/dt) may be caused by angular momentum loss due to magnetic stellar wind braking, while the cyclic period variations may be interpreted as LTTE terms induced by the presence of two additional bodies in the system, having masses of $M_3 \sin i_3 = 19.2\ M_{\rm J}$ and $M_4 \sin i_4 = 8.5\ M_{\rm J}$, respectively.[1] This model was independently tested by Beuermann et al. (2012), who found that it fails to fit their new eclipse timings and it is dynamically unstable on a time-scale of a few thousand years. Beuermann et al. also proposed a new LTTE model with two companions with masses of $M_3 \sin i_3 \simeq 14\ M_{\rm J}$ and $M_4 \sin i_4 = 30\text{-}120\ M_{\rm J}$, and periods of 12.7 and 55 ± 15 yr, respectively. Horner et al. (2012) independently tested Lee et al.'s model and came to the same conclusion about the dynamical instability of the system on very short time-scales; they also claimed that the ETVs cannot be driven by gravitational influence of perturbing planets only, and that there must be another astrophysical mechanism taking place in order to explain them.

Finally, Esmer et al. (2021) found a new two-planet solution, but it did not appear to be dynamically stable. The main differences between our approach and theirs will be summarized in the 'Discussion and Conclusions' section.

Regarding the Applegate effect, Navarrete et al. (2018) analysed the required energy to drive the Applegate effect in a sample of 12 close binary systems (including HW Vir), and compared it with the energy production of a simulated sample of magnetically active stars. In the case of HW Vir, they discarded the possibility of this effect being the underlying cause for the ETVs, since the magnetic field of the magnetically active star (i.e. the dM star) is not strong enough to produce these variations.

A conclusive explanation to HW Vir's ETVs is still missing. For this reason, our aim is to derive new eclipse timings from our unpublished photometric data, and use them along with the ones available in the literature to better constrain the physical parameters characterizing the system of HW Vir, as well as to test these new parameters for dynamical stability on a large time-scale.

The paper is organized as follows: In Section 2, we present our data, along with the data reduction process we followed, the light-curve fitting, and the determination of the eclipse timings, while in Section 4 we outline the LTTE modeling and test the previous model proposed to explain the ETVs of the system with our new data, as well as using an N-body integrator to test its dynamical stability. In Section 5, we describe the method we used to estimate new parameters for the putative companions of HW Vir. In Section 6, we discuss our findings and we draw some conclusions regarding the explanation behind the ETVs of HW Vir as well as some prospects for future work.

2 OBSERVATIONS AND DATA REDUCTION

Our analysed data set consists of 30 photometric observations of HW Vir obtained over time span of ∼11 yr (2008–2019), including 28 previously unpublished light curves. For our analysis, we combined data from five different instruments as described in the following.

From the Asiago Astrophysical Observatory located on Mt. Ekar in Asiago, we obtained 15 light curves using the 1.82 −m 'Copernico' telescope and the Asiago Faint Object Spectrograph and Camera. These images were taken with an exposure time ranging from 2 to 6 s, through the V, R, and r filters. Three light curves were obtained using the 67/92 − cm Schmidt telescope located at the same observatory. These observations were carried out in the R and r filters with an exposure time of 20 s, except for the last one (4 s).

Six light curves were obtained using the telescopes of the 'Gruppo Astrofili Salese Galileo Galilei';[2] the telescopes have a primary mirror with a diameter of 410 mm and a focal length of 1710 mm and they are located in Santa Maria di Sala, in Northern Italy. The observations were carried out in the V filter with an exposure time ranging from 20 to 45 s.

Our largest set in terms of number of data points comes from the Wide Angle Search for Planets (WASP-South; Pollacco et al. 2006), a transit survey with an array of small telescopes operating at the South African Astronomical Observatory (SAAO). WASP-South gathered four full seasons of observations of HW Vir from 2008 to 2012, for a grand total of 353 measured primary eclipses. This particular data

[1] $\sin i_3$ and $\sin i_4$ being the inclination with respect to the line of sight of the orbital plane of the inner and outer perturbers, respectively. Throughout this paper, we adopt this index convention, meaning the third and fourth massive bodies of the system.

[2] https://www.astrosalese.it/

Downloaded from https://academic.oup.com/mnras/article/506/2/2122/6313312 by INIST-CNRS INSU user on 20 April 2023

Table 1. Orbital and physical parameters of the components of HW Vir from the literature.

Parameter	Primary		Secondary	Reference
Orbital period P (d)		$0.116\,719\,67 \pm 1.15 \times 10^{-7}$		Beuermann et al. (2012)
Separation a ($R_\odot$)		0.860 ± 0.010		Lee et al. (2009)
Inclination i (°)		80.98 ± 0.10		Lee et al. (2009)
Eccentricity e		<0.0003		Beuermann et al. (2012)
Distance d (pc)		181 ± 20		Lee et al. (2009)
Mass ($M_\odot$)	0.485 ± 0.013		0.142 ± 0.004	Lee et al. (2009)
Radius ($R_\odot$)	0.183 ± 0.026		0.175 ± 0.026	Lee et al. (2009)
Temperature (K)	$28\,488 \pm 208$		3084 ± 889	Wood & Saffer (1999) and Lee et al. (2009)
Visual magnitude (V band)		10.6 (combined)	–	Zacharias et al. (2012)
Bolometric magnitude M_{bol} (mag)	1.46 ± 0.24		11.20 ± 0.46	Lee et al. (2009)
Absolute visual magnitude M_V (mag)	4.22 ± 0.24		15.59 ± 0.46	Lee et al. (2009)
Bolometric luminosity L_{bol} ($L_\odot$)	19.7 ± 5.6		0.003 ± 0.001	Lee et al. (2009)

Table 2. Log of observations. The columns give: a unique identifier (matching those in Fig. 1), the 'evening date' of the observation, the telescope used, the number of acquired frames, the photometric passband, and eclipses that were observed among the primary and secondary.

ID	'Evening' date	Telescope	N_{frames}	Filter	Phase coverage
w1-w4	2008–2012	WASP-South	18 410	WASP (clear)	Both (multiple)
s1	2012/03/11	Asiago Schmidt	321	*R*-Bessel	Both
s2	2012/03/12	Asiago Schmidt	332	*R*-Bessel	Both
s3	2018/04/20	Asiago Schmidt	557	*r*-Sloan	Primary
g1	2014/03/12	GAS	280	*V*-Bessel	Both
g2	2014/03/28	GAS	728	*V*-Bessel	Both twice
g3	2014/03/29	GAS	660	*V*-Bessel	Both twice
g4	2014/03/30	GAS	304	*V*-Bessel	Primary and partial secondary
g5	2014/03/31	GAS	700	*V*-Bessel	Both twice
g6	2014/05/24	GAS	325	*V*-Bessel	Both
c1	2011/02/05	Asiago 1.82-m	326	*R*-Bessel	Partial primary
c2	2012/01/26	Asiago 1.82-m	1392	*V*-Bessel	Both
c3	2013/02/04	Asiago 1.82-m	448	*V*-Bessel	Primary
c4	2013/02/07	Asiago 1.82-m	929	*V*-Bessel	Both
c5	2014/03/06	Asiago 1.82-m	1252	*V*-Bessel	Primary
c6	2014/04/01	Asiago 1.82-m	1086	*V*-Bessel	Primary
c7	2015/03/13	Asiago 1.82-m	320	*r*-Sloan	Partial primary
c8	2016/02/05	Asiago 1.82-m	620	*V*-Bessel	Primary
c9	2016/02/08	Asiago 1.82-m	1122	*V*-Bessel	Both
c10	2017/01/21	Asiago 1.82-m	1943	*r*-Sloan	Primary
c11	2017/02/25	Asiago 1.82-m	1663	*r*-Sloan	Both
c12	2017/03/02	Asiago 1.82-m	950	*r*-Sloan	Primary
c13	2019/01/03	Asiago 1.82-m	1632	*r*-Sloan	Both
c14	2019/03/12	Asiago 1.82-m	713	*r*-Sloan	Primary
c15	2019/03/31	Asiago 1.82-m	1170	*r*-Sloan	Both
kt1-2	2016	*K*2	89 970	*K*2 (clear)	Both (multiple)

set has not yet been included in a public data release, and has been kindly provided to us by the WASP-South team.

We also include in our analysis two light curves from *K*2 (Howell et al. 2014), observed during Campaign 10, and a vast collection of literature timings already analysed by Beuermann et al. (2012) and summarized at the end of this section. A detailed summary of all the observations is given in Table 2. Each light curve is identified with a unique ID with the leading letter matching the telescope: w for WASP-South, s for Asiago Schmidt, g for GAS, c for Asiago Copernico, and kt for *K*2. The w and kt light curves are split into four and two 'chunks' (respectively), for the reasons explained in Section 3.

Due to the lack of stellar crowding in the field of HW Vir, we use the differential aperture photometry technique to reduce our photometric series from the c, s, and g data sets. To perform the usual data reduction and the aperture photometry, we use the software STARSKY, a pipeline written in FORTRAN 77/90 by Nascimbeni et al. (2011, 2013), that was specially developed for The Asiago Search for Transit timing variations of Exoplanets (TASTE) project. As for the w data set, we take the light curves as they were delivered by the standard WASP software pipeline. For the *K*2 data, we extracted the light curve by reconstructing the 89 970 images containing HW Vir as done in Libralato et al. (2016), and performing a three-pixel aperture photometry of the target on each image, subtracting the local background measured in an annulus centred on the target and having radii $r_{in} = 7$ pixels and $r_{out} = 15$ pixels to the total flux. We detrended the light curve following the procedure by Nardiello

Downloaded from https://academic.oup.com/mnras/article/506/2/2122/6313312 by INIST-CNRS INSU user on 20 April 2023

et al. (2016). The resulting light curves from all the observations are shown in Fig. 1.

In order to measure timing variations with an absolute accuracy much better than 1 min, as needed for measuring ETVs, it is crucial to convert all our timestamps to a single, uniform time standard. Therefore, we convert all of them to the so-called Barycentric Julian Date computed from the Barycentric Dynamical Time, or BJD_{TDB}, following the prescription by Eastman, Siverd & Gaudi (2010). For this task, we rely on the `VARTOOLS` code.[3] Due to the crucial importance of this step for our dynamical analysis, we perform a double check of the conversion with the help of the online tool[4] made available by Eastman et al. (2010). We also apply this time conversion to all the 287 literature timings from SAAO, Wood, Zhang & Robinson (1993), Lee et al. (2009), BAV, VSNET, AAVSO, BRNO, and Beuermann et al. (2012), who, in turn, used timings from MONET/North. Again, all the HJD_{UTC} and BJD_{UTC} are homogeneously converted to BJD_{TDB} to ensure a proper comparison between the old timings and our new ones. A comprehensive listing of all the literature timings as converted by us is available in Appendix A.

3 ECLIPSE TIMINGS

To retrieve the best estimate of the orbital and physical parameters of the system, and most crucially the eclipse central time T_0, we fit an appropriate model to our light curves. For this purpose, we use the `JKTEBOP`[5] code (Southworth 2012), which was originally developed to fit light curves of detached eclipsing binaries and later adapted to model also exoplanetary transits. `JKTEBOP` implements non-linear least-squares optimization techniques [based on the Levenberg–Marquardt (LM) algorithm; Moré 1978]. It has different 'tasks' to choose from, according to how the light curves would be fitted and how the uncertainties are estimated. This process is meant to determine the best-fitting values of T_0 for each individual light curve and a reliable error estimate.

As a first step, we check that the software is properly fitting our light curves and converging to a physical solution by using `task3`, i.e. by simply running the task to each preliminary light curve and performing a visual inspection. At this stage, we decide to split the `w` and `kt` light curves into separate 'chunks'. For the WASP-South data, this is done because the composite light curve has a 4-yr coverage, and fitting it as a whole could in principle smear the LTTE signal; by splitting it into four distinct 'seasons' of about 4 months each, we completely avoid this risk (the shortest significant $O-C$ periodicity reported in the literature being ∼3000 d). As for the *K*2 data, the Campaign 10 light curve shows a large 2-week gap due to a repointing procedure followed by an unexpected shutdown of the camera. To make ourselves sure that there are no systematic errors introduced by this issue, we separately analysed the two chunks before and after the blank gap.

We then remove the outliers from our light curves at 4σ using `task4` of `JKTEBOP`, and, since we want to obtain a reliable measure of the eclipse time (T_0), we need to first build consistent templates of the parameters for each of the filters of our observations, to leave only T_0 as a free parameter in the final fit. To do this, we join the full-phase light curves from the same filter (since the light curves are colour dependent) and leave the following parameters free to find the best-fitting values: the sum of the stellar radii ($R_1 + R_2$), their ratio R_1/R_2, the inclination of their orbit, the surface brightness and the limb darkening of the primary star, the reflection coefficient of the secondary star, the scale factor, and the eclipse time (T_0). We do this for the *V* and *R*/*r* filters, and additionally, for the WASP and *K*2 light curves. Then, we run `task9` of `JKTEBOP`, which uses a *residual-shift* method to obtain the best fit. This method evaluates the best fit for the data points and shifts the residuals of the fit point by point through all the data, calculating a new best fit after each shift. This approach allows us to have as many best fits as points in the input light curve, and it also estimates the relevance of the correlated red noise to the parameters of the fit. The output of this task is therefore three high-accuracy parameter sets (templates), one for each filter: a *V* template for the Copernico/*V* and GAS light curves; an *R*/*r* template for the Copernico/*R*, *r* and the Schmidt/*R* light curves; and an unfiltered template for the WASP and *K*2 light curves.

We retrieve the T_0s by running `task9` one more time, fixing all the parameters except the eclipse times. An example of the quality of the fit on our two most complete light curves from the Copernico telescope (`c2` in Bessel *V* and `c11` in Sloan *r*) is shown in Fig. 2.

The resulting timings of HW Vir are reported in Table 3. We compute a total of 30 mid-eclipse timings, with an excellent median timing error for our light curves of only ∼1.3 s and down to 0.3 s for the best ones (from the `c` and `w` sets). Our new data increase the current number of high-precision observations [$\sigma(T_0) < 5$ s] by about 50 per cent, and extend the baseline by 6 yr with respect to the dynamical study of HW Vir (Beuermann et al. 2012).

We build the observed minus calculated ($O-C$) diagram for HW Vir by plotting both the new and old eclipse timings as a function of the epoch *E*, using the linear ephemeris formula derived by Beuermann et al. (2012), by fitting their mid-eclipse times alone:

$$T_c = 2455\,543.984\,055(2) + 0.116\,719\,555(2) \times E, \quad (1)$$

where T_c is the calculated time of the primary eclipse in the BJD_{TDB} time standard. In Fig. 3, we show the $O-C$ diagram including all the up-to-date eclipse timings of HW Vir. As it can be seen, our new data match the existing one with a remarkable precision (within 1σ), which also serves as an external check for our absolute time calibration.

4 MODELLING

4.1 LTTE calculation

To calculate the LTTE, we develop a `FORTRAN 77` code that implements an adaptation of the equation by Irwin (1952) to compute the LTTE:

$$\tau_k = K_k \left[\frac{1-e_k^2}{1+e_k \cos \upsilon_k} \sin(\upsilon_k + \omega_k) \right], \quad (2)$$

where the subindex $k = 1, 2, \ldots$ indicates the stellar or substellar companion causing the modulation, τ_k is the light-time delay, e_k is the eccentricity of the orbit, ω_k is the argument of periastron, υ_k is the true anomaly, and K_k is the semi-amplitude of the modulation given by

$$K_k = \frac{a_{k,\mathrm{bin}} \sin i_k}{c}, \quad (3)$$

where $a_{k\,\mathrm{bin}}$ is the semimajor axis of the orbit of the binary around the common centre of mass, i_k is the inclination of the orbit with respect to the line of sight, and *c* is the speed of light.

[3] https://www.astro.princeton.edu/~jhartman/vartools
[4] http://astroutils.astronomy.ohio-state.edu/time/
[5] http://www.astro.keele.ac.uk/jkt/codes/jktebop.html

Downloaded from https://academic.oup.com/mnras/article/506/2/2122/6313312 by INIST-CNRS INSU user on 20 April 2023

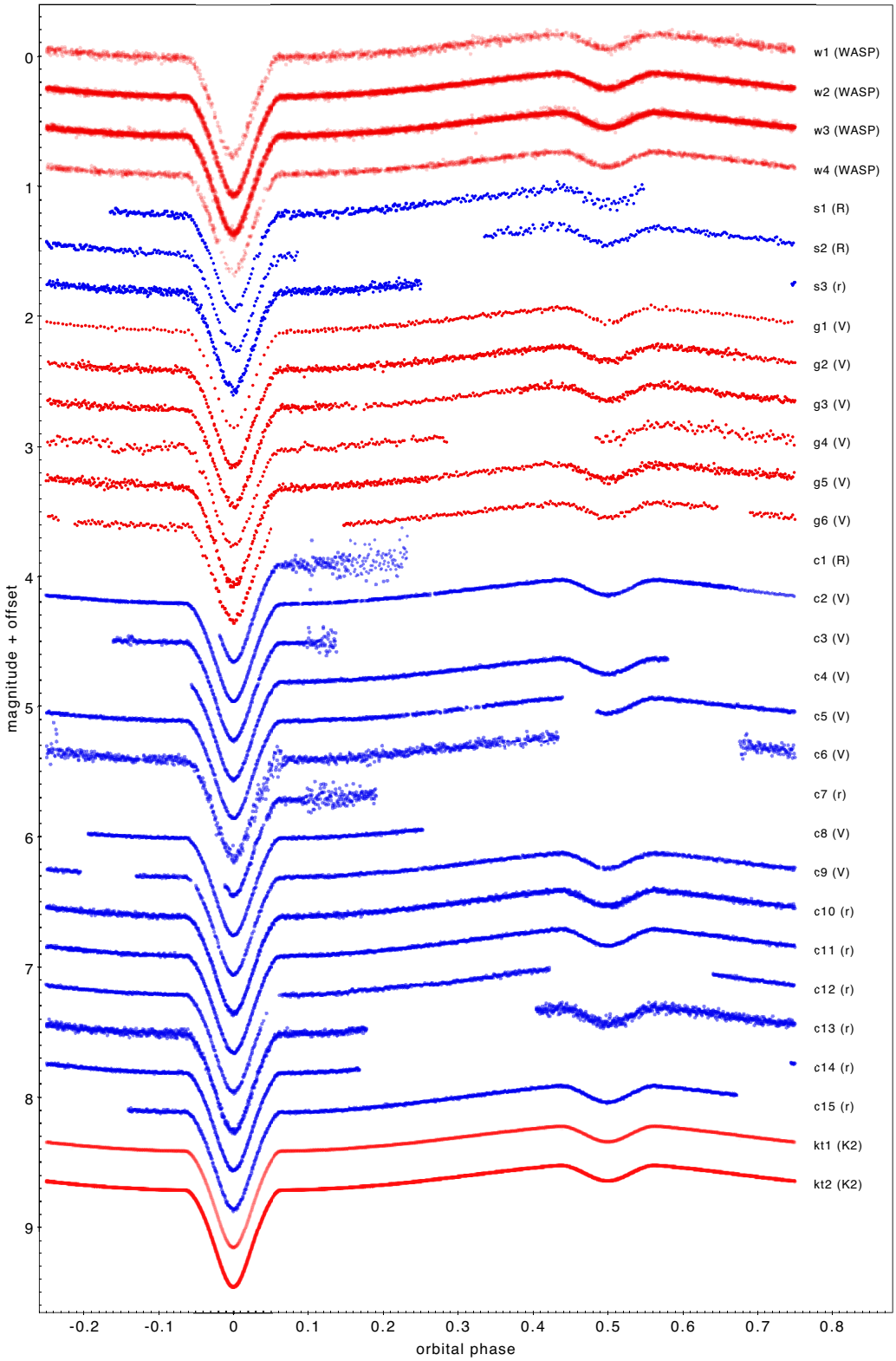

Figure 1. The 30 light curves of HW Vir analysed in this study, plotted as a function of the orbital phase. Each curve is labelled with an identifier (matching those in Table 2) and the filter name (uppercase for the Bessel system, lowercase for SDSS). The SuperWASP (`w1-w4`) and *K*2 (`kt1-kt2`) curves are split into separate chunks as described in Section 3. The colour scheme is used for visual reference to identify each set of light curves.

Downloaded from https://academic.oup.com/mnras/article/506/2/2122/6313312 by INIST-CNRS INSU user on 20 April 2023

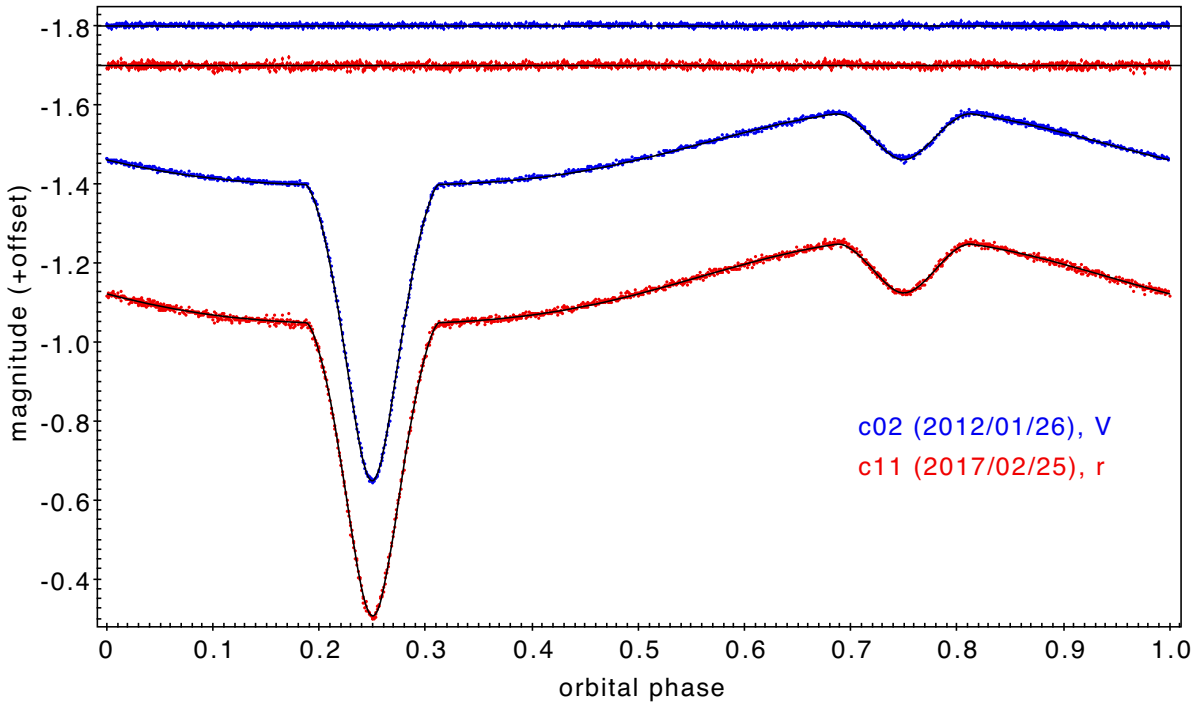

Figure 2. JKTEBOP best-fitting models on our two most complete light curves from the Copernico telescope: `c2` in Bessel *V* (blue points) and `c11` in Sloan *r* (red points). The residuals are shown in the upper part of the plot; their rms scatter is 3.1 and 5.0 mmag, respectively.

The approach of Irwin (1952) was to use the plane perpendicular to the line of sight that passes through the centre of the elliptical orbit of the binary about the centre of mass of all the bodies in the system as the reference frame, which adds a $ne_k \sin\omega_k$ term to equation (2). Our approach is to use another perpendicular (and parallel) plane to the line of sight that passes through the centre of mass of all the bodies in the system as the reference frame, resulting in the exclusion of this term.

4.2 Test of the previous model

By fitting a model with the contribution of two LTTE terms (τ, described in Section 1), Beuermann et al. (2012) derived an underlying linear ephemeris for the binary given by

$$T_c = 2455\,730.550\,186(3) + 0.116\,719\,675(6) \times E. \quad (4)$$

To test this two-companion model, we plot the $O - C$ diagram using both the literature data and our new eclipse timings in Fig. 4. The model is able to reproduce the data from the literature very well; however, it fails to fit our new data.

We check the dynamical stability of this model by reproducing the same test performed by Beuermann et al. (2012) using the `MERCURY6`[6] (Chambers 1999) package. We set the initial Keplerian parameters of the system with the binary as a single body of mass $M_{\rm bin} = M_1 + M_2$ at the centre of the system, as described in Beuermann et al. (2012), and we use the same hybrid symplectic integrator. As a first test, we integrate for 10^4 yr, and we find that the inner planet is ejected after ∼2500 yr, in contrast with Beuermann et al. (2012)'s paper, who suggest that their proposed model is stable for 10^8 yr.

We perform additional checks using the `radau` integrator within the `MERCURY6` code, and also using the `PYTHON-C` package `rebound`[7] (Rein & Liu 2012) with three of their different integrators namely, `ias15` (Rein & Spiegel 2015), `whfast` (Rein & Tamayo 2015), and `mercurius`. All the simulations were run for 10^6 yr, using a step size of 8.8 d (1/530 of P_3) with output every 308.9 d (1/15 of P_3). Additionally, we test the stability with a new version of `MERCURY6`, `MERCURY6_binary`,[8] a modified version of the original code by Smullen, Kratter & Shannon (2016), which allows us to simulate both single and binary stars, treating the central star in the binary as a composite 'big body' instead of a single central object. Following the advise by the author, we use the `radau` integrator to perform the simulation, and we integrate for 10^6 yr with the same step size described above. We consider a planet to escape or be ejected at a distance >150 au.

The initial orbital and physical parameters used for all the simulations performed are listed in Table 4. The results of all the simulations returned unstable systems, in different time-scales and for different reasons, such as ejection of outer or inner planet, a close encounter between planets, or the inner planet colliding with the binary. As a final check, we use the Mean Exponential Growth factor of Nearby Orbits (MEGNO; Cincotta & Simó 2000) indicator in `rebound`. Briefly, the MEGNO indicator $\langle Y \rangle$ will reach the value of $\langle Y \rangle = 2$ for stable orbits, and it will be $\langle Y \rangle \gg 2$ for unstable configurations (in the case of $\langle Y \rangle > 4$ or a close encounter and an ejection, we assign the maximum value $\langle Y \rangle = 4$). We set the initial conditions as in Table 4, but we let vary, for the inner companion (identified with the subindex 3), the semimajor axis a_3 from 1 to 6 au and the eccentricity e_3 from 0 to 0.5, both in 100 linear steps. We

[6]We used the version available at https://github.com/4xxi/mercury.

[7]https://rebound.readthedocs.io/en/latest/

[8]https://github.com/rsmullen/mercury6_binary

Downloaded from https://academic.oup.com/mnras/article/506/2/2122/6313312 by INIST-CNRS INSU user on 20 April 2023

Table 3. Best-fitting eclipse timings (T_0) for the primary eclipse of HW Vir derived from our unpublished data. The epoch is computed with respect to the linear ephemeris in equation (1).

T_0 (BJD$_{TDB}$)	σ_{T_0} (d)	Epoch	ID
2455598.608756	0.000 039	468	c1
2455953.669686	0.000 004	3510	c2
2456328.572882	0.000 004	6722	c3
2456331.607585	0.000 007	6748	c4
2456723.551785	0.000 006	10 106	c5
2456749.463503	0.000 022	10 328	c6
2457095.536914	0.000 035	13 293	c7
2457424.685857	0.000 003	16 113	c8
2457427.603842	0.000 006	16 138	c9
2457775.661358	0.000 010	19 120	c10
2457810.560486	0.000 007	19 419	c11
2457815.579418	0.000 009	19 462	c12
2458487.650169	0.000 014	25 220	c13
2458555.580938	0.000 003	25 802	c14
2458574.372776	0.000 008	25 963	c15
2455998.606687	0.000 022	3895	s1
2455999.657099	0.000 048	3904	s2
2458229.466702	0.000 026	23 008	s3
2456729.504448	0.000 022	10 157	g1
2456745.495025	0.000 015	10 294	g2
2456746.428763	0.000 023	10 302	g3
2456747.479294	0.000 050	10 311	g4
2456748.413045	0.000 025	10 319	g5
2456802.454163	0.000 046	10 782	g6
2454539.612655	0.000 012	−8605	w1
2454961.436853	0.000 003	−4991	w2
2455283.582736	0.000 004	−2231	w3
2455596.741284	0.000 008	452	w4
2457584.4748480	0.000 0003	17 482	kt1
2457629.1784108	0.000 0002	17 865	kt2

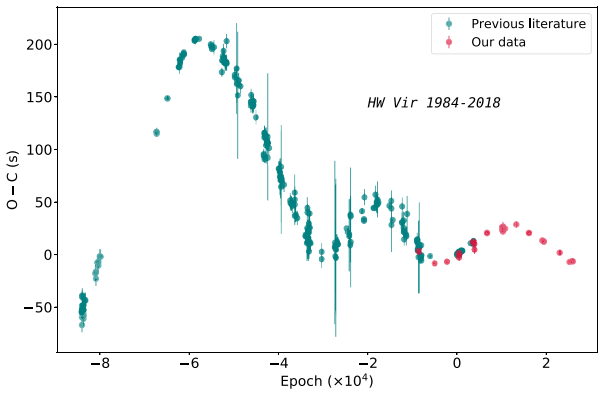

Figure 3. $O - C$ T_0 diagram of HW Vir built with the literature data plus our data. We use equation (1) to obtain the linear ephemeris (T_c; see the text) and compute the $O - C$.

compute the orbits of each configuration with the `whfast` integrator with a step size of 1 d for an integration time of 10^5 yr. The final grid has 100 000 simulations, each returning a MEGNO value. As shown in Fig. 5, we find that the solution from Beuermann et al. (2012), depicted by the red dot, lies on an unstable region, confirming our tests with different codes and integrators. It is worth noting that all the simulations have the same reference frame as in Winn (2010),

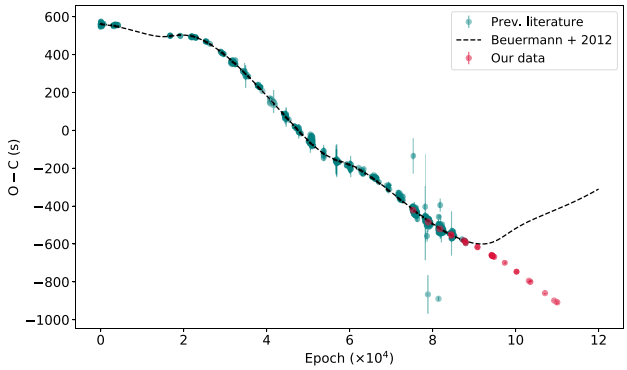

Figure 4. $O - C$ diagram of HW Vir showing Beuermann et al.'s model along with all the literature timings available, with the model extended along time and our new timings overplotted for comparison. Some of the error bars fall within the size of the points. We use equation (4) to obtain the linear ephemeris and to compute the $O - C$.

Table 4. Orbital and physical parameters of HW Vir and the two companions proposed by Beuermann et al. (2012) used for the dynamical stability tests, where the subscripts bin, 3, and 4 represent the binary, and the inner and outer companions, respectively. Values marked with ∗ are assumed values.

Parameter	Value
M_{bin}	0.627 $M_\odot$
R_{bin}	0.860 $R_\odot$
M_3	14.3 M_J
R_3∗	1 R_J
a_3	4.69 au
e_3	0.4
i_3	80.9°
ω_3	−18°
$\mathcal{M}_3$	33°
Ω_3	180°
M_4	65 M_J
R_4∗	2 R_J
a_4	12.8 au
e_4	0.05
i_4	80.9°
ω_4	0°
$\mathcal{M}_4$	166.23°
Ω_4	180°

which is the plane X–Y in the sky plane and $\Omega_{3,4} = 180°$, and we assume the orbits to be coplanar with the binary.

5 A NEW MODEL

Our aim at this stage is to find a new LTTE model that properly fits the data. We separately analysed two data sets: one with all the available data (317 points), and one for which we discarded the first two observing seasons from the literature (35 photoelectric measurements between JD 2445730 and 2445745 from Kilkenny et al. 1994). From now on, we will refer to these data sets as the 'full' and the 'reduced' one, respectively. The latter selection was done as a test since the Kilkenny et al. (1994) data were always suspiciously offset from any best-fitting model and lack the original time-series data; i.e. we are unable to perform any independent check on them. We also rescale all the T_0 errors by adding in quadrature 1 s to Beuermann et al. (2012)'s and our values, and 5 s to the rest of the literature values. We apply this rescaling to take into account

Downloaded from https://academic.oup.com/mnras/article/506/2/2122/6313312 by INIST-CNRS INSU user on 20 April 2023

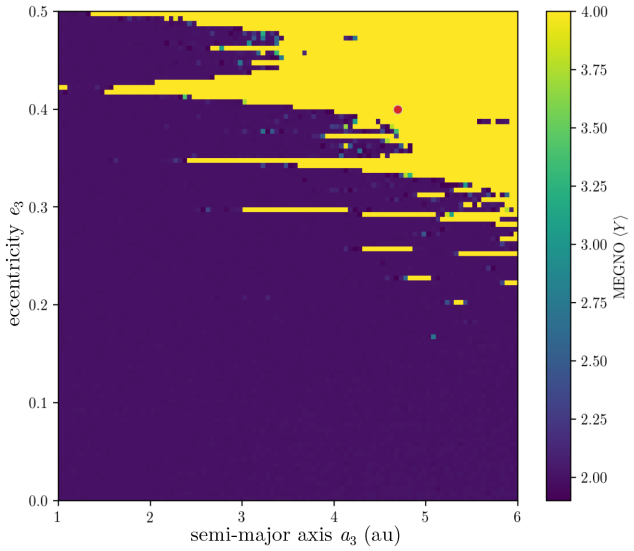

Figure 5. MEGNO values, $\langle Y \rangle$, of each simulation based on Beuermann et al. (2012)'s solution with varying a_3 (1–6 au) and e_3 (0–0.5). To the simulations that did not complete the orbital integration or that returned $\langle Y \rangle > 4$, we assigned $\langle Y \rangle = 4$ (unstable). The configuration of Beuermann et al. (2012) is unstable and it is shown as the red dot (overplotted on the yellow region).

systematic errors in the absolute calibration of the timestamps at this level (due for instance to clock drift, to the finite shutter traveltime, or to technical dead times while commanding the camera or saving the images). This assumption will be later empirically justified by the residual of our best-fitting models being very close to $\chi^2_r \simeq 1$.

After removing the outliers and rescaling the errors, we extend the code described in Section 4.1 with the implementation of `PIKAIA` (Charbonneau 1995), a genetic algorithm to solve multimodal optimization problems. This algorithm is based on the theory of evolution by means of natural selection; that is, a new population is generated by choosing the fittest pairs from the original population, and this process continues until a certain fitness level is achieved or after a pre-defined number of generations. We perform 100 000 simulations of 1000 generations each on a population of 200 individuals and we use the inverse of the reduced chi-square $1/\chi^2_r$ as our fitness function. Once the code computes the results for `PIKAIA` at the end of each simulation, it uses the LM algorithm to refine the `PIKAIA` output and it calculates the final best-fitting solution.

We also run an independent analysis based on a modified version of `PIKAIA` in `FORTRAN 90`, wrapped in `PYTHON`, and coupled with the affine invariant ensemble sampler (Goodman & Weare 2010) algorithm implemented in the `EMCEE` package (Foreman-Mackey et al. 2013). The `PIKAIA` part used 200 individuals (a set of parameters) for 2000 generations, while we run `EMCEE` with 100 walkers (or chains) for 10000 steps (we remove the initial 2000 steps as burn-in). We repeat this coupled analysis 1000 times.

The same fitting parameters are used in both approaches, that is a linear ephemeris with reference time $T_{\rm ref}$ and period $P_{\rm bin}$, and the LTTE parameters for each k-th body, i.e. $a_{k\,\rm bin}\sin i$, period P_k, eccentricity e_k, argument of pericentre ω_k, and the time of the passage at pericentre $t_{{\rm peri},\,k}$. We use the same boundaries of the fitting parameters for this code and the previous one (see Table 5). All the parameters have uniform uninformative priors.

We obtain a large set of solutions, but we select only the solutions that, first, are physically meaningful (i.e. we discard negative eccentricity solutions, since LM is not bounded in the parameter intervals),

Table 5. Boundaries of the parameters of linear ephemeris plus two LTTE models.

Parameter	Min.	Max.
$T_{\rm ref}$ (BJD$_{\rm TDB}$)	2445 730.5	2445 730.6
$P_{\rm bin}$ (d)	0.116 719	0.116 723
$a_{3\,\rm bin}\sin i$ (au)	0	1
P_3 (d)	2000	10 000
e_3	0	0.5
ω_3 (°)	0	360
$t_{\rm peri\,3}$ (d)	2452 000	2465 000
$a_{4\,\rm bin}\sin i$ (au)	0.5	5
P_4 (d)	10 000	40 000
e_4	0	0.7
ω_4 (°)	0	360
$t_{{\rm peri},\,4}$ (d)	2452 000	2491 000

and have a $\chi^2_r < 2$. For each of these selected simulations, we run a stability[9] check with `rebound` and the MEGNO indicator. We run simulations for 10^5 yr with the `whfast` integrator and a small step size of 1 d. We apply the full analysis (model fitting with two approaches and stability analysis) and find that all the solutions with $\chi^2_r < 2$ are unstable for both data sets.

We show in Fig. 6 the $O - C$ diagram for the two-companion model for the four best solutions (lowest χ^2_r) for both PIKAIA implementations and both data sets. The four solutions show clearly different contributions from the inner (3) and outer (4) companions, with different periods, amplitudes, and patterns; yet, they fit the observed data points surprisingly well, especially on the 'reduced' data set. It is worth noting that both solutions on the full data set are not able to properly reproduce the general trend of the two observing seasons around epoch 20 000 (1989–1990), being forced to fit the earliest points by Kilkenny et al. (1994).

In Table 6, we present the orbital and physical parameters of these best-fitting solutions. Values for the masses of the companions are within the brown dwarf range. We did not attempt to compute realistic errors (i.e. other than the nominal errors output from the LM fit) on the derived parameters due to the dynamical instability of all the solutions we found.

Additionally, we test a different model with a linear ephemeris ($T_{\rm c}$), a one-companion LTTE (τ_3), and a quadratic term (Q). We apply this model to both data sets only with the `PIKAIA + EMCEE` approach. We use uniform priors within the boundaries in Table 7. We find solutions with $\chi^2_r > 6$ (see Table 7 and Fig. 7) and Bayesian Information Criteria that are higher than the two-companion model, for both the data sets. For this reason, we discard this model as a possible explanation for the ETVs.

6 DISCUSSION AND CONCLUSIONS

In this work, we presented a study of the eclipsing binary system HW Vir by using hitherto unpublished photometric observations from four different facilities. We converted all the light curve timings into a common reference frame, as it was crucial for the purposes of this work to have accurate and homogeneous timestamps in order to properly compare different data sets. By combining our new

[9]We compute the mass of the k-th companion by combining the third Kepler's law and $a_{k,\,\rm bin} = a_k M_k/(M_k + M_{\rm bin})$ and finding the real root of a polynomial of third order in M_k of kind $M_k^3 - x M_k^2 - 2x M_{\rm bin} M_k - x M_{\rm bin}^2 = 0$ with $x = \frac{4\pi^2}{G}\frac{a_{k,\rm bin}^3}{P_k^2}$ and $k = 3$ and 4.

Downloaded from https://academic.oup.com/mnras/article/506/2/2122/6313312 by INIST-CNRS INSU user on 20 April 2023

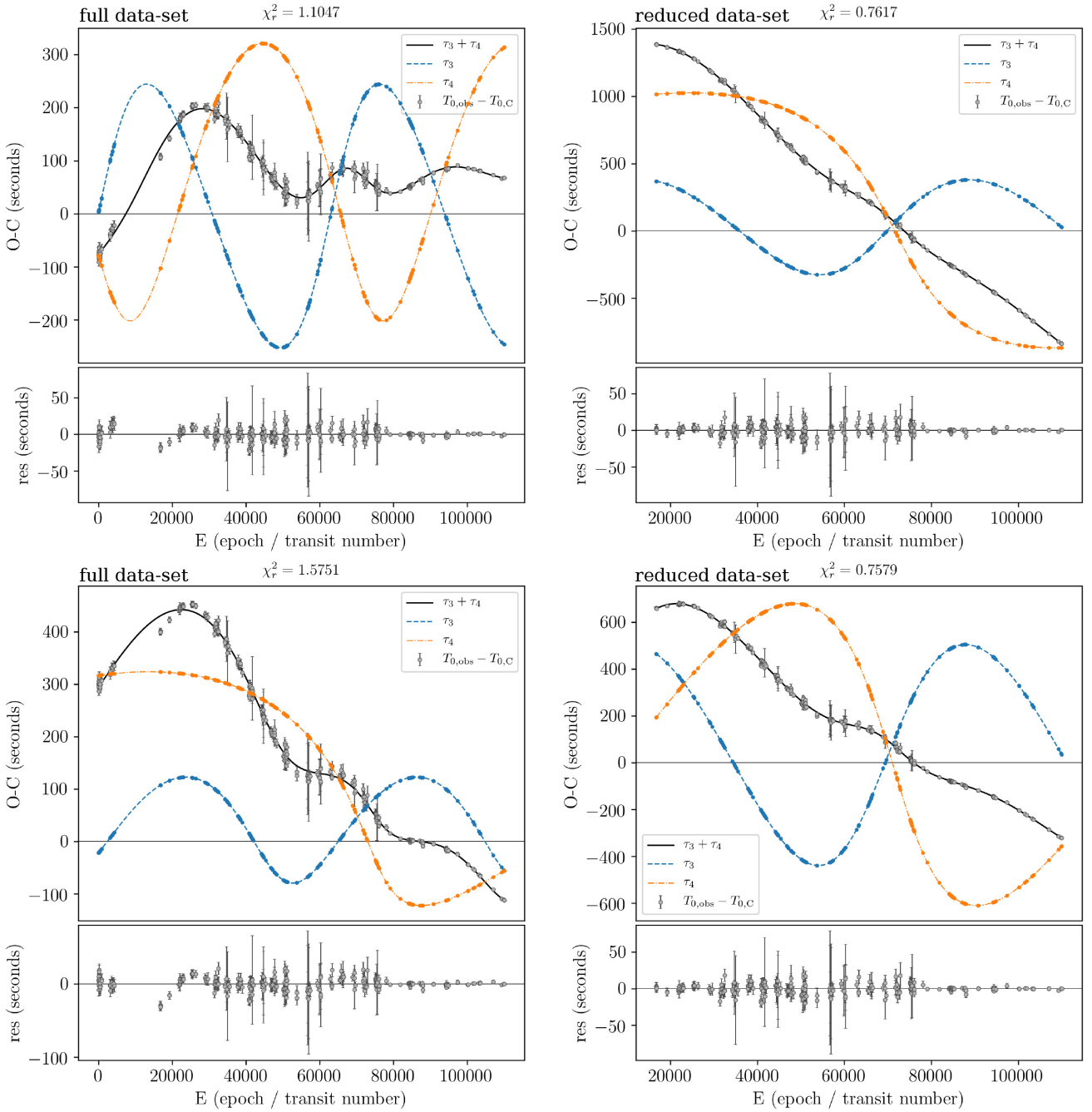

Figure 6. The best two-companion models as the result of the fit to the full data set (left column) and the reduced data set (right column) from the best-fitting solution of the PIKAIA + LM (upper row) and of the PIKAIA + EMCEE (lower row) code. For each solution, we show in the upper panel the $O - C$ (grey dots) as observed eclipse times ($T_{0\,\mathrm{obs}}$) minus the linear ephemeris ($T_{0\,\mathrm{c}}$), the combined LTTE of the two companions ($\tau_3 + \tau_4$ as black line), and the single LTTE of the companions (τ_3 and τ_4 as blue dashed line and orange dash–dotted line, respectively). The lower panel shows the residuals as $T_{0\,\mathrm{obs}} - (T_{0\,\mathrm{c}} + \tau_3 + \tau_4)$.

timings with the ones available in the literature, we independently confirmed that the Beuermann et al. (2012) model reproduces the recent literature data until 2011, but it is unable to fit our new timings. Additionally, we tested the dynamical stability of their proposed model and we found it to be unstable after only a few thousand years, opposite to their claim of 10^8 yr of stability.

As a first effort to find a proper model for the LTTE in HW Vir, we used the PIKAIA code, which implements a genetic algorithm to explore the parameter space and estimate new parameters for the companions of the binary system. We found a set of parameter vectors with a very good fit in a statistical sense, able to explain all the available data. Notwithstanding, these sets of solutions led to very high values for the masses of the companions of HW Vir ($\sim 50 M_J$, within the mass range of brown dwarfs) and dynamically unstable systems.

Regarding the recent work of Esmer et al. (2021), we describe the most significant differences between their approach and ours in the following. We performed a fully homogeneous analysis of all the new light curves presented, with the same tools and by fitting an accurate EB model (rather than measuring the T_0s with the Kwee &

Downloaded from https://academic.oup.com/mnras/article/506/2/2122/6313312 by INIST-CNRS INSU user on 20 April 2023

Table 6. Orbital and physical parameters of our four best-fitting solutions for the ETVs of HW Vir with two-companion model.

Model and physical parameters	Full data set		Reduced data set	
	PIKAIA + LM	PIKAIA + EMCEE	PIKAIA + LM	PIKAIA + EMCEE
$T_{\rm ref}^{(a)}$ (BJD$_{\rm TDB}$)	45 730.557 572	45 730.553 198	45 730.538 213	45 730.549 2131
$P_{\rm bin}$ (d)	0.116 7195	0.116 7196	0.116 7198	0.116 7196
$a_{3,\,\rm bin}\sin i$ (au)	0.51	0.20	0.72	0.96
P_3 (d)	7367	7315	8781	8947
e_3	0.235	0.241	0.159	0.199
ω_3 (°)	4	242	331	340
$t_{\rm peri,3}^{(a)}$ (BJD$_{\rm TDB}$)	60 499	58 757	62 135	53 506
$a_3\sin i^{(b)}$ (au)	6.5	6.4	7.4	7.6
$M_3^{(b)}$ (M$_{\rm J}$)	56	22	70	96
$a_{4,\,\rm bin}\sin i$ (au)	0.53	0.56	2.58	1.45
P_4 (days)	8 012	26 155	34 258	13 649
e_4	0.24	0.7	0.68	0.445
ω_4 (°)	251	211	185	186
$t_{\rm peri,4}^{(a)}$ (BJD$_{\rm TDB}$)	70 449	54 541	54 160	54 103
$a_4\sin i^{(b)}$ (au)	6.9	15	18.6	10.1
$M_4^{(b)}$ (M$_{\rm J}$)	54	26	106	110
$\chi^2_{\rm r}$	1.105	1.575	0.762	0.758
dof	258	227	258	227

[a] BJD$_{\rm TDB}$ −2400000.
[b] Physical parameter computed from the model parameters.

Table 7. Boundaries and best-fitting parameters of the one-companion model ($T_{\rm c} + \tau_3 + Q$).

Parameter	Min.	Max.	Best fit	
			Full data set	Reduced data set
$T_{\rm ref}$ (BJD$_{\rm TDB}$)	2445 730.5	2445 730.6	2445 730.557 5759	2445 730.555 9335
$P_{\rm bin}$ (d)	0.116 719	0.116 723	0.116 7196	0.116 7197
$a_{3,\,\rm bin}\sin i$ (au)	0	1	0.213	0.295
P_3 (d)	500	50 000	9750	10 396
e_3	0	0.5	0.41	0.37
ω_3 (°)	0	360	123	116
$t_{\rm peri,\,3}$ (d)	2452 000	2502 000	2459 013	2459 294
Q	-10^{-8}	10^{-8}	-7.1×10^{-13}	-1.2×10^{-12}
$\chi^2_{\rm r}$			6.868	7.520
dof			262	231

van Woerden 1956 method; Li et al. 2018). This, coupled with the use of larger telescopes, resulted in more accurate eclipse timings by a factor of 5, on average. Also, we exploited a genetic algorithm to perform a comprehensive global search of the parameter space rather than a local one. For this reason, although our search for stable LTTE orbits has been unfruitful, the orbital parameters of our four new solutions fall well outside the region explored by Esmer et al. (2021). The direct $O-C$ comparison of their T_0 with ours is also reassuring, as the average offsets of the residuals measured on a season-by-season basis demonstrate the subsecond accuracy in the absolute timestamp calibration of both data sets.

Although the best-fitting solutions we found were proven to be dynamically unstable, it is worth asking whether other stable orbital solutions with similar LTTE amplitudes exist, and how could we confirm or disprove them with one or more independent techniques.

The prospects for a follow-up with *direct imaging* are not very promising in the short term. The combination of angular separation (in our best solution, 0.″11 and 0.″47, respectively) and contrast ($\simeq10^{-5}$ in the K band if we assume the typical luminosity of a mature 50 $M_{\rm J}$ brown dwarf; Phillips et al. 2020) falls beyond or very close to the sensitivity limits of the existing ground-based facilities such as SPHERE (Spectro-Polarimetric High-contrast Exoplanet REsearch; Beuzit et al. 2019) and GPI (Gemini Planet Imager; Ruffio et al. 2017). However, such systems may become very interesting targets for upcoming high-contrast imaging missions such as *JWST* and *the Roman Space Telescope*.

On the other hand, *astrometry* as a follow-up approach could be much more feasible with the release in the near future of the individual astrometric measurements by *GAIA* (*Gaia* Collaboration 2016). If we assume that the observed $O-C$ is entirely due to a combination of LTTE signals, its amplitude A_{O-C} can be easily translated into the expected astrometric signal, s, as $s = A_{O-C}\times c/d$, where d is the distance to HW Vir from Table 1. We probe a range of A_{O-C} from 100 to 1500 s, which is spanning the amplitude of the oscillating LTTE terms of the orbital solutions claimed in the recent literature and also compatible with those included in our two best-fitting models in Fig. 6. We find that s ranges from 1.10 ± 0.12 to 16.6 ± 1.8 mas for $A_{O-C} = 100$ and 1500 s, respectively. That is in principle comfortably within the reach of *GAIA* sensitivity, since the expected astrometric precision of the individual positional measurements of HW Vir is ∼30 μas (Sahlmann, Triaud & Martin 2015). In such a scenario, the detection will be limited by the temporal baseline rather than the astrometric precision. Yet, if *Gaia* will survive up to its operational goal of 10 yr, at least the LTTE component with the shortest period can be robustly retrieved, while

Downloaded from https://academic.oup.com/mnras/article/506/2/2122/6313312 by INIST-CNRS INSU user on 20 April 2023

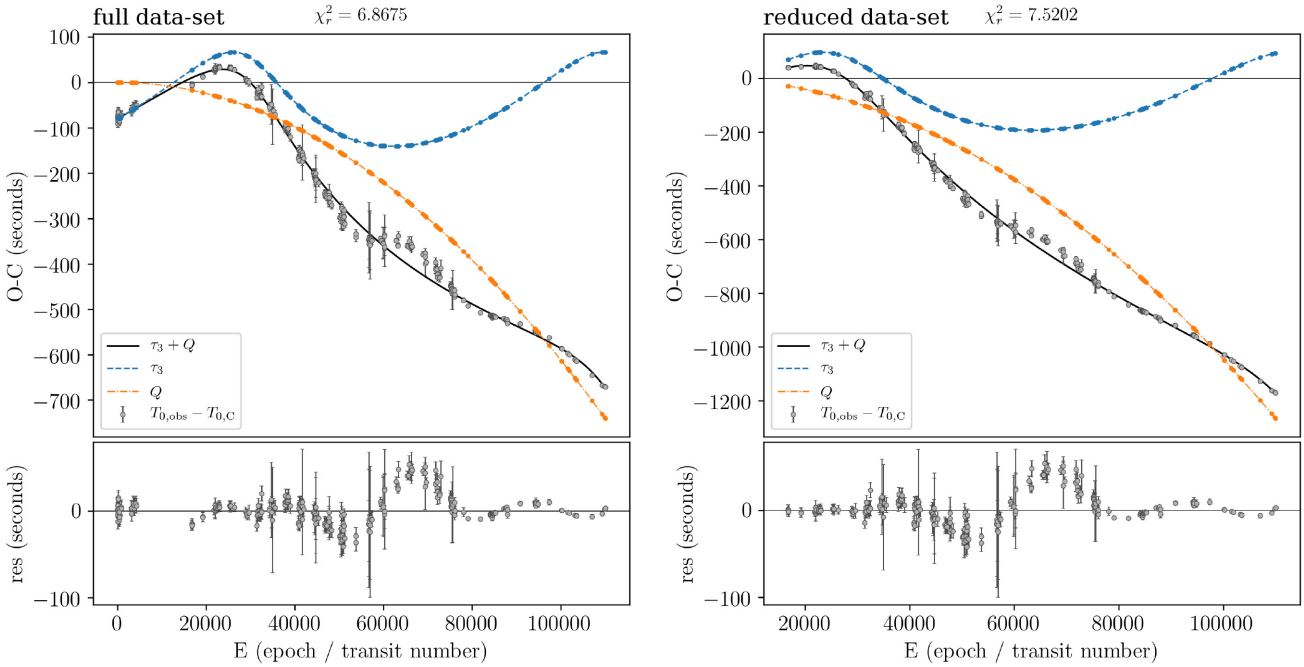

Figure 7. The best one-companion models as the result of the fit to the full data set (left) and the reduced data set (right). Similar to Fig. 6, but now displaying the Q term instead of τ_4. The lower panel shows the residuals as $T_{0\,\mathrm{obs}} - (T_{0\,\mathrm{c}} + \tau_3 + Q)$. Due to the high χ^2_r, these models are not suitable to explain the ETVs of HW Vir.

for the longest one a global analysis combining *Gaia* with the existing ETV data points will be needed.

A satisfying explanation for the ETVs of HW Vir is still eluding us; however, this only highlights the fact that there is still a lot to be learned about systems of this kind. One of the challenges to accurately determine the underlying cause of the ETVs in this case is that the observations show that the period of one of the components from the LTTE of HW Vir is longer than the total observational time span available. Therefore, increasing the observational baseline will certainly bring us closer to determine the cause behind the ETVs of HW Vir.

ACKNOWLEDGEMENTS

GP and LB acknowledge the funding support from Italian Space Agency (ASI) regulated by 'Accordo ASI-INAF n. 2013-016-R.0 del 9 luglio 2013 e integrazione del 9 luglio 2015 CHEOPS Fasi A/B/C'. LT acknowledges support from Ministero dell'Università e della Ricerca (MIUR; PRIN 2017 grant 20179ZF5KS). DN acknowledges the support from the French Centre National d'Etudes Spatiales (CNES).

DATA AVAILABILITY

The data underlying this article will be uploaded on Vizier/CDS in a second stage; in the meantime, it will be shared on reasonable request to the corresponding author.

REFERENCES

Applegate J. H., 1992, ApJ, 385, 621
Beuermann K., Dreizler S., Hessman F. V., Deller J., 2012, A&A, 543, A138
Beuzit J. L. et al., 2019, A&A, 631, A155
Bours M. C. P. et al., 2016, MNRAS, 460, 3873
Brewer J. M., Wang S., Fischer D. A., Foreman-Mackey D., 2018, ApJ, 867, L3
Çakirli Ö., Devlen A., 1999, A&AS, 136, 27
Chambers J. E., 1999, MNRAS, 304, 793
Charbonneau P., 1995, ApJS, 101, 309
Cincotta P. M., Simó C., 2000, A&AS, 147, 205
Eastman J., Siverd R., Gaudi B. S., 2010, PASP, 122, 935
Esmer E. M., Baştürk Ö., Hinse T. C., Selam S. O., Correia A. C. M., 2021, A&A, 648, A85
Foreman-Mackey D., Hogg D. W., Lang D., Goodman J., 2013, PASP, 125, 306
Gaia Collaboration et al., 2016, A&A, 595, A1
Gillon M. et al., 2017, Nature, 542, 456
Goodman J., Weare J., 2010, Commun. Appl. Math. Comput. Sci., 5, 65
Gould A. et al., 2014, Science, 345, 46
Heber U., 2016, PASP, 128, 082001
Horner J., Hinse T. C., Wittenmyer R. A., Marshall J. P., Tinney C. G., 2012, MNRAS, 427, 2812
Howell S. B. et al., 2014, PASP, 126, 398
İbanoğlu C., Çakırlı Ö., Taş G., Evren S., 2004, A&A, 414, 1043
Irwin J. B., 1952, ApJ, 116, 211
Kilkenny D., Marang F., Menzies J. W., 1994, MNRAS, 267, 535
Kilkenny D., Keuris S., Marang F., Roberts G., van Wyk F., Ogloza W., 2000, The Observatory, 120, 48
Kilkenny D., van Wyk F., Marang F., 2003, The Observatory, 123, 31
Kiss L. L., Csák B., Szatmáry K., Furész G., Sziládi K., 2000, A&A, 364, 199
Konacki M., Muterspaugh M. W., Kulkarni S. R., Hełminiak K. G., 2009, ApJ, 704, 513
Kostov V. B. et al., 2016, ApJ, 827, 86
Kwee K. K., van Woerden H., 1956, Bull. Astron. Inst. Neth., 12, 327
Lee J. W., Kim S.-L., Kim C.-H., Koch R. H., Lee C.-U., Kim H.-I., Park J.-H., 2009, AJ, 137, 3181
Li M. C. A. et al., 2018, MNRAS, 480, 4557
Libralato M., Bedin L. R., Nardiello D., Piotto G., 2016, MNRAS, 456, 1137
Mayor M., Queloz D., 1995, Nature, 378, 355
Menzies J. W., Marang F., 1986, in Hearnshaw J. B., Cottrell P. L., eds, Proc. IAU Symp. 118, Instrumentation and Research Programmes for Small Telescopes. D. Reidel Publishing Company, Dordrecht, Holland. Norwell, MA, p. 305

Downloaded from https://academic.oup.com/mnras/article/506/2/2122/6313312 by INIST-CNRS INSU user on 20 April 2023

Moré J. J., 1978, The Levenberg–Marquardt Algorithm: Implementation and Theory. Springer Verlag. Berlin,p. 105
Nardiello D., Libralato M., Bedin L. R., Piotto G., Borsato L., Granata V., Malavolta L., Nascimbeni V., 2016, MNRAS, 463, 1831
Nascimbeni V., Piotto G., Bedin L. R., Damasso M., 2011, A&A, 527, A85
Nascimbeni V. et al., 2013, A&A, 549, A30
Navarrete F. H., Schleicher D. R. G., Zamponi J., Völschow M., 2018, A&A, 615, A81
Petigura E., Marcy G. W., Howard A., 2015, American Astronomical Society Meeting Abstracts, 225, 406.03
Phillips M. W. et al., 2020, A&A, 637, A38
Pollacco D. L. et al., 2006, PASP, 118, 1407
Rein H., Liu S. F., 2012, A&A, 537, A128
Rein H., Spiegel D. S., 2015, MNRAS, 446, 1424
Rein H., Tamayo D., 2015, MNRAS, 452, 376
Ruffio J.-B. et al., 2017, ApJ, 842, 14
Sahlmann J., Triaud A. H. M. J., Martin D. V., 2015, MNRAS, 447, 287
Sale O., Bogensberger D., Clarke F., Lynas-Gray A. E., 2020, MNRAS, 499, 3071
Silvotti R. et al., 2018, A&A, 611, A85
Smullen R. A., Kratter K. M., Shannon A., 2016, MNRAS, 461, 1288
Southworth J., 2012, Astrophysics Source Code Library, record ascl:1207.013
Winn J. N., 2010, Exoplanet Transits and Occultations. University of Arizona Press, Tucson, AZ,p. 55
Wolszczan A., Frail D. A., 1992, Nature, 355, 145
Wood J. H., Saffer R., 1999, MNRAS, 305, 820
Wood J. H., Zhang E.-H., Robinson E. L., 1993, MNRAS, 261, 103
Zacharias N., Finch C. T., Girard T. M., Henden A., Bartlett J. L., Monet D. G., Zacharias M. I., 2013, AJ, 145, 14

APPENDIX A: LITERATURE TIMINGS

In this table, we list the 240 timing measurements taken from the literature (from the compilation by Kilkenny et al. 1994, K94; Lee et al. 2009, L09; Beuermann et al. 2012, B12) and included in our fits together with our new data (Table 3), after being converted by us into a uniform BJD_{TDB} time standard (Eastman et al. 2010). The epoch is computed according to the ephemeris in equation (1) of (Beuermann et al. 2012).

Table A1. Literature eclipse times for HW Vir.

T_0 (BJD_{TDB})	$\sigma(T_0)$	Epoch	Reference
2445730.556669	.000 099	0	K94
2445731.607139	.000 099	9	K94
2445732.540889	.000 099	17	K94
2445733.591389	.000 099	26	K94
2445734.525149	.000 099	34	K94
2445735.575549	.000 099	43	K94
2445736.509219	.000 099	51	K94
2445740.477899	.000 099	85	K94
2445740.594559	.000 099	86	K94
2445741.528339	.000 099	94	K94
2445742.462240	.000 099	102	K94
2445744.446450	.000 099	119	K94
2445773.509431	.000 099	368	K94
2445773.626191	.000 099	369	K94
2445774.443131	.000 099	376	K94
2445774.559881	.000 099	377	K94
2445775.376921	.000 099	384	K94
2445775.610421	.000 099	386	K94
2445776.427511	.000 099	393	K94
2445776.544181	.000 099	394	K94
2445819.380354	.000 099	761	K94
2445823.932404	.000 099	800	K94
2446086.551616	.000 099	3050	K94
2446098.573736	.000 099	3153	K94
2446100.557976	.000 099	3170	K94
2446101.608376	.000 099	3179	K94
2446139.075518	.000 099	3500	K94
2446164.403620	.000 099	3717	K94
2446164.520380	.000 099	3718	K94
2446203.271322	.000 099	4050	K94
2446223.347073	.000 099	4222	K94
2447684.326630	.000 065	16 739	L09
2447687.244620	.000 065	16 764	L09
2447688.295090	.000 076	16 773	L09
2447689.228830	.000 065	16 781	L09
2447968.539023	.000 061	19 174	L09
2447972.507483	.000 061	19 208	L09
2448267.574765	.000 061	21 736	L09
2448294.887134	.000 099	21 970	L09
2448295.003934	.000 099	21 971	L09
2448295.937624	.000 099	21 979	L09
2448307.609604	.000 061	22 079	L09
2448311.578084	.000 061	22 113	L09
2448313.562324	.000 061	22 130	L09
2448365.385823	.000 059	22 574	L09
2448371.455263	.000 059	22 626	L09
2448404.370202	.000 059	22 908	L09
2448406.354412	.000 065	22 925	L09
2448410.322872	.000 061	22 959	L09
2448682.512946	.000 061	25 291	L09
2448684.497166	.000 059	25 308	L09
2448703.522456	.000 076	25 471	L09
2448704.456226	.000 059	25 479	L09
2448705.506696	.000 059	25 488	L09
2448803.317656	.000 059	26 326	L09
2449104.453947	.000 065	28 906	L09
2449122.312007	.000 061	29 059	L09
2449137.368797	.000 061	29 188	L09
2449139.353057	.000 059	29 205	L09
2449190.242759	.000 099	29 641	L09
2449393.567882	.000 076	31 383	L09
2449400.571182	.000 076	31 443	L09
2449418.546033	.000 099	31 597	L09
2449427.533383	.000 076	31 674	L09
2449437.571373	.000 099	31 760	L09
2449450.643884	.000 099	31 872	L09
2449476.322135	.000 099	32 092	L09
2449480.407315	.000 099	32 127	L09
2449485.309515	.000 099	32 169	L09
2449511.337986	.000 099	32 392	L09
2449518.341386	.000 099	32 452	L09
2449519.274896	.000 099	32 460	L09
2449728.552864	.000 099	34 253	L09
2449733.571774	.000 099	34 296	L09
2449778.625606	.000 503	34 682	L09
2449785.628606	.000 208	34 742	L09
2449808.505507	.000 702	34 938	L09
2449833.483648	.000 099	35 152	L09
2449880.288110	.000 099	35 553	L09
2450142.556692	.000 099	37 800	L09
2450144.540882	.000 099	37 817	L09
2450147.575632	.000 099	37 843	L09
2450155.512633	.000 091	37 911	L09
2450185.392715	.000 099	38 167	L09
2450186.443205	.000 099	38 176	L09
2450201.383275	.000 099	38 304	L09
2450202.433755	.000 099	38 313	L09

Downloaded from https://academic.oup.com/mnras/article/506/2/2122/6313312 by INIST-CNRS INSU user on 20 April 2023

Table A1 – *continued*

T_0 (BJD$_{TDB}$)	$\sigma(T_0)$	Epoch	Reference
2450216.673546	.000 099	38 435	L09
2450218.424376	.000 099	38 450	L09
2450222.509566	.000 099	38 485	L09
2450280.285549	.000 099	38 980	L09
2450491.430748	.000 083	40 789	L09
2450491.547448	.000 076	40 790	L09
2450506.487748	.000 099	40 918	L09
2450509.522508	.000 099	40 944	L09
2450510.572978	.000 099	40 953	L09
2450511.506448	.000 070	40 961	L09
2450511.506728	.000 099	40 961	L09
2450543.721290	.000 099	41 237	L09
2450547.456320	.000 099	41 269	L09
2450547.689760	.000 099	41 271	L09
2450552.475150	.000 208	41 312	L09
2450575.468952	.000 099	41 509	L09
2450594.377552	.000 702	41 671	L09
2450595.427952	.000 099	41 680	L09
2450596.361552	.000 099	41 688	L09
2450597.295462	.000 099	41 696	L09
2450599.279703	.000 099	41 713	L09
2450600.330183	.000 099	41 722	L09
2450631.260795	.000 099	41 987	L09
2450883.491443	.000 099	44 148	L09
2450885.475673	.000 099	44 165	L09
2450910.453614	.000 099	44 379	L09
2450912.321074	.000 208	44 395	L09
2450912.554564	.000 099	44 397	L09
2450927.494574	.000 208	44 525	L09
2450931.346364	.000 099	44 558	L09
2450943.368574	.000 116	44 661	L09
2450943.485074	.000 208	44 662	L09
2450946.403174	.000 503	44 687	L09
2450948.387375	.000 603	44 704	L09
2450955.390545	.000 099	44 764	L09
2450959.242275	.000 099	44 797	L09
2451021.220295	.000 099	45 328	L09
2451183.576969	.000 099	46 719	L09
2451190.580109	.000 099	46 779	L09
2451216.491839	.000 099	47 001	L09
2451236.567569	.000 099	47 173	L09
2451300.413290	.000 208	47 720	L09
2451301.346790	.000116	47 728	L09
2451301.463690	.000 116	47 729	L09
2451302.397390	.000 208	47 737	L09
2451326.324779	.000 099	47 942	L09
2451368.227049	.000 099	48 301	L09
2451578.555416	.000 099	50 103	L09
2451582.523896	.000 099	50 137	L09
2451608.552335	.000 099	50 360	L09
2451616.489185	.000 208	50 428	L09
2451627.460985	.000 345	50 522	L09
2451630.145755	.000 070	50 545	L09
2451630.262425	.000 070	50 546	L09
2451654.423084	.000 208	50 753	L09
2451655.356784	.000 208	50 761	L09
2451668.429584	.000 099	50 873	L09
2451671.463984	.000 099	50 899	L09
2451674.382184	.000 208	50 924	L09
2451688.038573	.000 076	51 041	L09
2451689.088893	.000 124	51 050	L09
2451691.423283	.000 116	51 070	L09
2451692.356883	.000 116	51 078	L09
2451712.315903	.000 099	51 249	L09

Table A1 – *continued*

T_0 (BJD$_{TDB}$)	$\sigma(T_0)$	Epoch	Reference
2452001.429972	.000 116	53 726	L09
2452001.546772	.000 116	53 727	L09
2452342.251085	.000 059	56 646	L09
2452348.437235	.000 712	56 699	L09
2452348.553995	.000 902	56 700	L09
2452349.487705	.000 099	56 708	L09
2452353.456065	.000 404	56 742	L09
2452356.490895	.000 099	56 768	L09
2452373.298454	.000 722	56 912	L09
2452373.415084	.000 872	56 913	L09
2452402.361703	.000 099	57 161	L09
2452410.298603	.000 099	57 229	L09
2452431.308112	.000 099	57 409	L09
2452650.390821	.000 061	59 286	L09
2452675.368760	.000 065	59 500	L09
2452724.390928	.000 394	59 920	L09
2452724.507628	.000 394	59 921	L09
2452756.371957	.000 070	60 194	L09
2452759.406997	.000 523	60 220	L09
2452764.425637	.000 503	60 263	L09
2452764.542637	.000 208	60 264	L09
2453061.360425	.000 065	62 807	L09
2453112.716925	.000 059	63 247	L09
2453112.833625	.000 061	63 248	L09
2453124.972714	.000 107	63 352	L09
2453360.746019	.000 059	65 372	L09
2453384.323359	.000 059	65 574	L09
2453410.702118	.000 116	65 800	L09
2453444.083818	.000 116	66 086	L09
2453444.200518	.000 116	66 087	L09
2453465.443518	.000 208	66 269	L09
2453466.377218	.000 116	66 277	L09
2453491.355218	.000 076	66 491	L09
2453773.933130	.000 059	68 912	L09
2453825.289771	.000 061	69 352	L09
2453829.024531	.000 306	69 384	L09
2453829.141431	.000 208	69 385	L09
2453861.589331	.000 059	69 663	L09
2454105.182936	.000 116	71 750	L09
2454108.217636	.000 116	71 776	L09
2454108.334536	.000 116	71 777	L09
2454143.233437	.000 116	72 076	L09
2454143.350237	.000 116	72 077	L09
2454155.255507	.000 059	72 179	L09
2454155.372217	.000 059	72 180	L09
2454158.290127	.000 091	72 205	L09
2454214.082109	.000 065	72 683	L09
2454216.416479	.000 116	72 703	L09
2454239.410470	.000 208	72 900	L09
2454498.877648	.000 116	75 123	L09
2454498.877674	.000 060	75 123	B12
2454509.148988	.000 065	75 211	L09
2454509.265688	.000 059	75 212	L09
2454512.300308	.000 059	75 238	L09
2454513.350858	.000 083	75 247	L09
2454514.167808	.000 059	75 254	L09
2454514.284538	.000 059	75 255	L09
2454515.335018	.000 065	75 264	L09
2454517.319248	.000 059	75 281	L09
2454533.193149	.000 116	75 417	L09
2454533.309849	.000 116	75 418	L09
2454535.177249	.000 404	75 434	L09
2454554.902950	.000 503	75 603	L09
2454588.401364	.000 070	75 890	B12

Downloaded from https://academic.oup.com/mnras/article/506/2/2122/6313312 by INIST-CNRS INSU user on 20 April 2023

Table A1 – *continued*

T_0 (BJD_{TDB})	$\sigma(T_0)$	Epoch	Reference
2454601.707367	.000 060	76 004	B12
2454607.076602	.000 065	76 050	L09
2454608.593786	.000 061	76 063	B12
2454611.628553	.000 059	76 089	B12
2454841.916149	.000 059	78 062	B12
2455543.984048	.000 014	84 077	B12
2455549.003005	.000 014	84120	B12
2455556.006176	.000 015	84180	B12
2455582.968393	.000 015	84 411	B12
2455584.952622	.000 015	84 428	B12
2455591.955807	.000 015	84 488	B12
2455593.006274	.000 014	84 497	B12
2455605.028372	.000 014	84 600	B12
2455605.962117	.000 019	84 608	B12
2455615.883298	.000 014	84 693	B12
2455635.725619	.000 013	84 863	B12
2455647.864460	.000 014	84 967	B12
2455648.914932	.000 014	84 976	B12
2455654.750921	.000 013	85 026	B12
2455680.779371	.000 014	85 249	B12
2455682.763597	.000 019	85 266	B12
2455896.010239	.000 014	87 093	B12
2455953.903110	.000 021	87 589	B12
2455957.988315	.000 014	87 624	B12
2455977.013609	.000 014	87 787	B12

This paper has been typeset from a TEX/LATEX file prepared by the author.

Downloaded from https://academic.oup.com/mnras/article/506/2/2122/6313312 by INIST-CNRS INSU user on 20 April 2023